Journal of Metastable and Nanocrystalline Materials
ISSN: 2297-6620, Vol. 31, pp 43-50
doi:10.4028/www.scientific.net/JMNM.31.43

Submitted: 2017-12-30
Accepted: 2018-03-18
Online: 2019-01-15

Characterization of the Superelastic and Structural Characteristics of β-Ti Alloys by Strain-Controlled Cycling after Thermomechanical Processing and Subsequent Ageing

V. Sheremetyev[1,a*], M.F. Ijaz[1,b], A. Kudryashova[1,c], A. Konopatsky[1,d], S. Prokoshkin[1,e], V. Brailovski[1f]

[1]National University of Science and Technology "MISIS", Leninskiy prosp. 4, Moscow 119049, Russia

[2]Ecole de Technologie Superieure,1100, Notre-Dame Str. West, Montreal (Quebec), H3C 1K3, Canada

[a]sheremetyev@misis.ru, [b]farzik98@gmail.com, [c]nastya.cudriaschova@yandex.ru, [d]ankonopatsky@gmail.com, [e]prokoshkin@tmo.misis.ru, [f]Vladimir.Brailovski@etsmtl.ca

Keywords: shape memory alloys, thermomechanical treatments, martensitic transformations, stress hysteresis, strain-controlled tensile tests, superelasticity, room temperature ageing

Abstract. In this comparative study, the structural and superelastic characteristics of two thermomechanically treated metastable Ti-Nb based (Ti-22Nb-6Zr) and Ti-Zr based (Ti-18Zr-14Nb and Ti-18Zr-13Nb-2Ta (at. %)) alloy systems were studied. To study the influence of room temperature storage on the functional properties of these two alloy systems, the alloys were subjected to a multistage testing routine consisting of four ten-cycle loading-unloading testing series alternated with three room temperature ageing periods (1, 5 and 20 days). Based on microstructure-properties relationships, it was shown that for each alloy system, the forward stress-induced martensitic transformation was essentially dependent on the material microstructure, whereas the subsequent reverse martenstic transformation was controlled by the material composition. The Ti-Zr based alloys demonstrated more stable functional behavior than their Ti-Nb based counterparts. More specifically Ti-18Zr-13Nb-2Ta, subjected to a combination of cyclic training alternated with room temperature ageing showed a significant improvement in superelastic behavior with small accumulated strains and narrow stress hysteresis.

Introduction

Metastable β-type Ti-Nb and Ti-Zr based shape memory alloys (SMA) are regarded as excellent candidates for medical implants because they exhibit a unique combination of biomechanical compatibility (highly-compliant plateau-like hysteretic behavior) and biochemical compatibility (high corrosion resistance in body fluids). While the biomechanical compatibility of these alloys is associated with their superelastic behavior mimicking the mechanical behavior of bone tissues, the biochemical compatibility for its part is associated with the non-toxic compositional design of these alloys [1-5]. Considering the application of β-Ti alloys as load-bearing implant materials, the assessment of their functional fatigue behavior constitutes a mandatory step [3, 5].

Fundamentally, the superelasticity of Ti-Nb and Ti-Zr based alloys during conventional mechanical cycling is attributed to stress-induced forward $\beta \rightarrow \alpha''$ and reverse $\alpha'' \rightarrow \beta$ martensitic transformations [6]. Ultimately, during fatigue cycling, the magnitude of stress hysteresis ($\Delta\sigma_{\beta \leftrightarrow \alpha''}$) originating from the $\beta \leftrightarrow \alpha''$ stress-controlled transformation plays a key role in governing/controlling the overall superelastic characteristics of β-type Ti-Nb and Ti-Zr based alloys [7-9]. Indeed, it is argued that tuning the $\Delta\sigma_{\beta \leftrightarrow \alpha''}$ of β-type Ti alloys by compositional design and/or thermomechanical treatments constitutes a useful strategy for the enhancement of their functional cyclic stability [2, 3, 7, 10].

To date, no comparative analysis has been reported revealing the impact of mechanical cycling after room temperature ageing on the stress-strain behavior of the recently developed β-type Ti-Nb and Ti-Zr based alloys. Hence, in this study, a systematic investigation showing the effect of room

temperature ageing on the room temperature superelastic behavior of metastable Ti-22Nb-6Zr [1], Ti-18Zr-14Nb [2] and Ti-18Zr-13Nb-2Ta [11] (at.% hereinafter) alloys has been carried out.

1. Experimental

In this work, 40 g ingots of three metastable alloys: Ti-22Nb-6Zr (TNZ), Ti-18Zr-14Nb (TZN) and Ti-18Zr-13Nb-2Ta (TZNT) were produced by vacuum arc remelting with a non-consumable tungsten electrode under argon protective atmosphere. For each ingot, the remelting process was repeated five times to reach chemical and structural homogeneity, and the ingots were turned upside down after each remelting. The preparatory melting of pure titanium provided low amounts of impurities (O<0.06, C<0.04, N<0.0008, H<0.010 wt.%). Crystallization was carried out in a water-cooled copper mold. The ingots were then EDM-cut in 1×1.5×50-mm specimens and subjected to thermomechanical treatment (TMT) including cold rolling (CR) with a true logarithmic strain of e=0.3 and post-deformation annealing (PDA) at 600°C (30 min) followed by water cooling.

This TMT aimed to form a nano- and/or submicro-subgrained structure in β-phase and create conditions for room temperature superelasticity [11, 12]. For X-ray diffraction analysis, the TMT-processed specimens were mechanically polished and etched in 3HF:6HNO3:12H2O solution to remove a damaged surface layer.

The first series of 10-cycle loading-unloading strain-controlled tensile tests (strain of up to ε=2% in each cycle) were performed on 40 mm-gauge length samples, using an "MTS MiniBionox" tensile testing machine. After one-day RT-ageing, the second series of 10-cycle testing was conducted, followed by 5-day RT-ageing, the third series of 10-cycle testing, 20-day RT-aging, and the fourth series of 10-cycle testing (Fig. 1). In all control points from 1 to 5 (Fig. 1), the phase constituents were analyzed using X-ray diffraction analysis ("PANalytical X'Pert Pro" diffractometer). The lattice parameters of the studied phases were calculated from the angular coordinates of the β and α'' XRD peaks. Where possible, the maximum $\beta \rightleftarrows \alpha''$ transformation lattice strain (εmax), which corresponds to a theoretical recovery strain limit, was calculated from the lattice parameters of the α'' and β-phases. The calculation procedure was based on the least-square method and the extrapolation of the β-phase lattice parameters to θ=90°, as described in [13, 14].

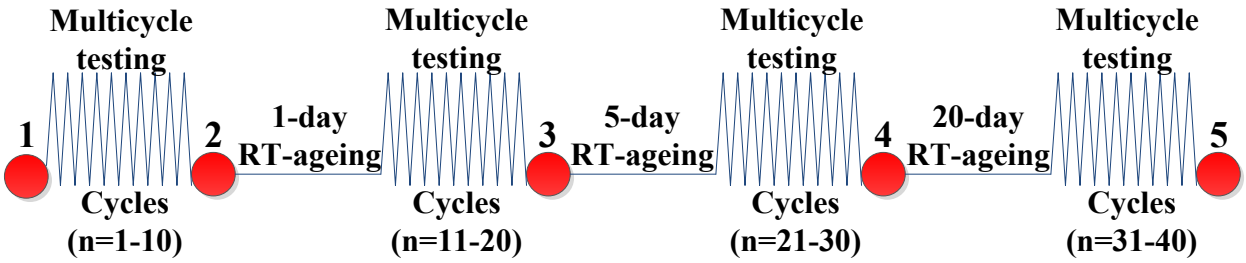

Fig. 1. Experimental schedule; points 1 to 5 are control points for X-ray diffractometry analysis.

2. Results and Discussion

2.1 Evolution of superelastic behavior

The results of the four-stage strain-controlled cyclic tensile tests of metastable TNZ, TZN and TZNT alloys are shown in Fig. 2. The TNZ and TZNT alloys manifested non-perfect superelastic behavior during the initial cycling stage, which transformed to perfect superelasticity in the course of the first cycling series (n=1-10). Conversely, the TZN alloy started to demonstrate perfect superelasticity only during the second cycling stage (n=11-20). It should however be noted, that conditions for perfect room temperature superelasticity are less conducive for the TNZ than for the TZN and TZNT alloys, apparently due to a significantly higher Ms temperature in the former [10].

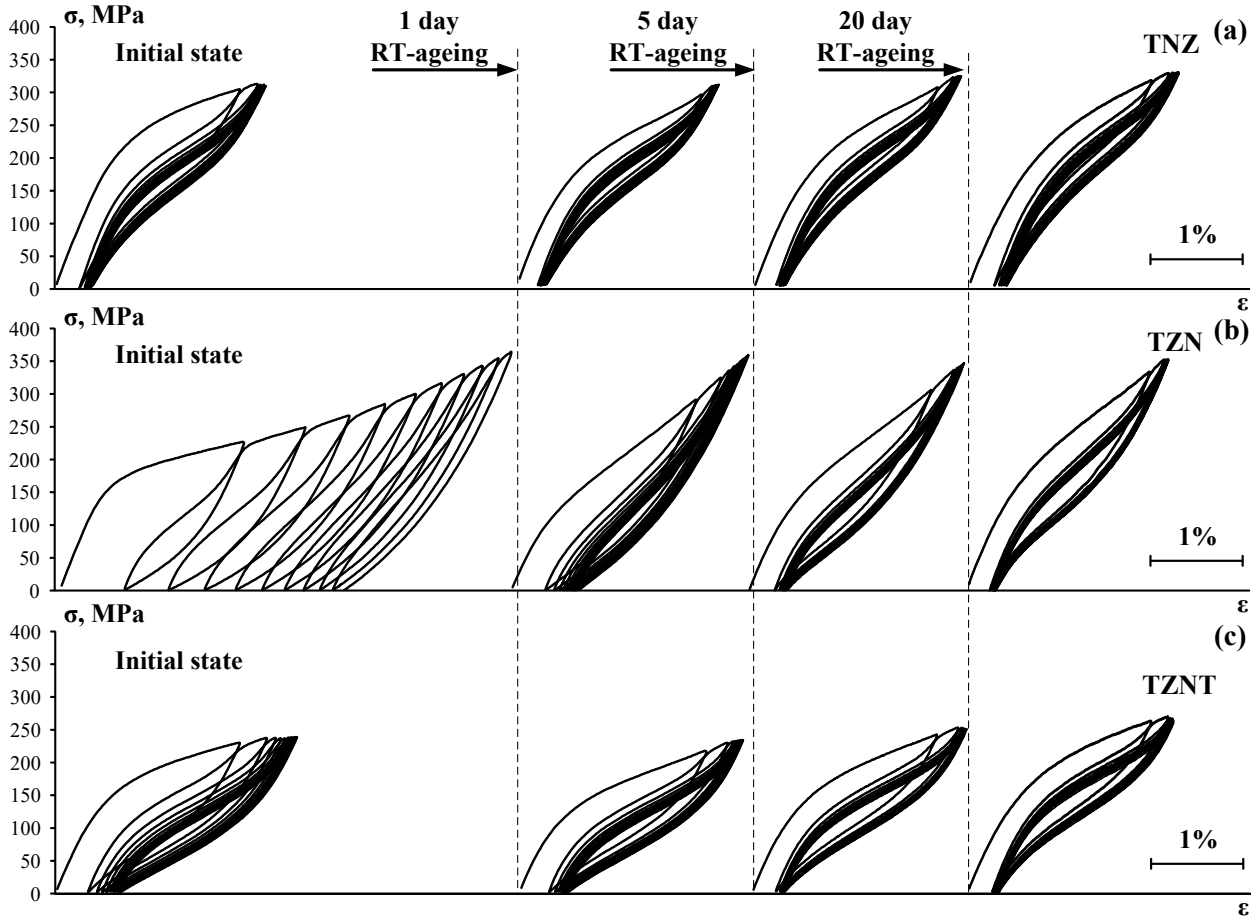

Fig. 2. Evolution of the loading-unloading diagrams of the (a) TNZ, (b) TZN and (c) TZNT alloys.

To characterize the functional properties quantitatively, the following parameters of the stress-strain diagrams were evaluated (Fig. 3a): the stress at which martensitic transformation starts ($\sigma_{\beta\rightarrow\alpha''}$), the stress at which reverse martensitic transformation ends ($\sigma_{\alpha''\rightarrow\beta}$), the corresponding stress hysteresis ($\Delta\sigma_{\beta\leftrightarrow\alpha''}$), the "engineering" (apparent) Young's modulus (E), and the accumulated residual strain (ε_{acc}). These parameters are also plotted against each cycle number, as shown in Fig. 3(b-f).

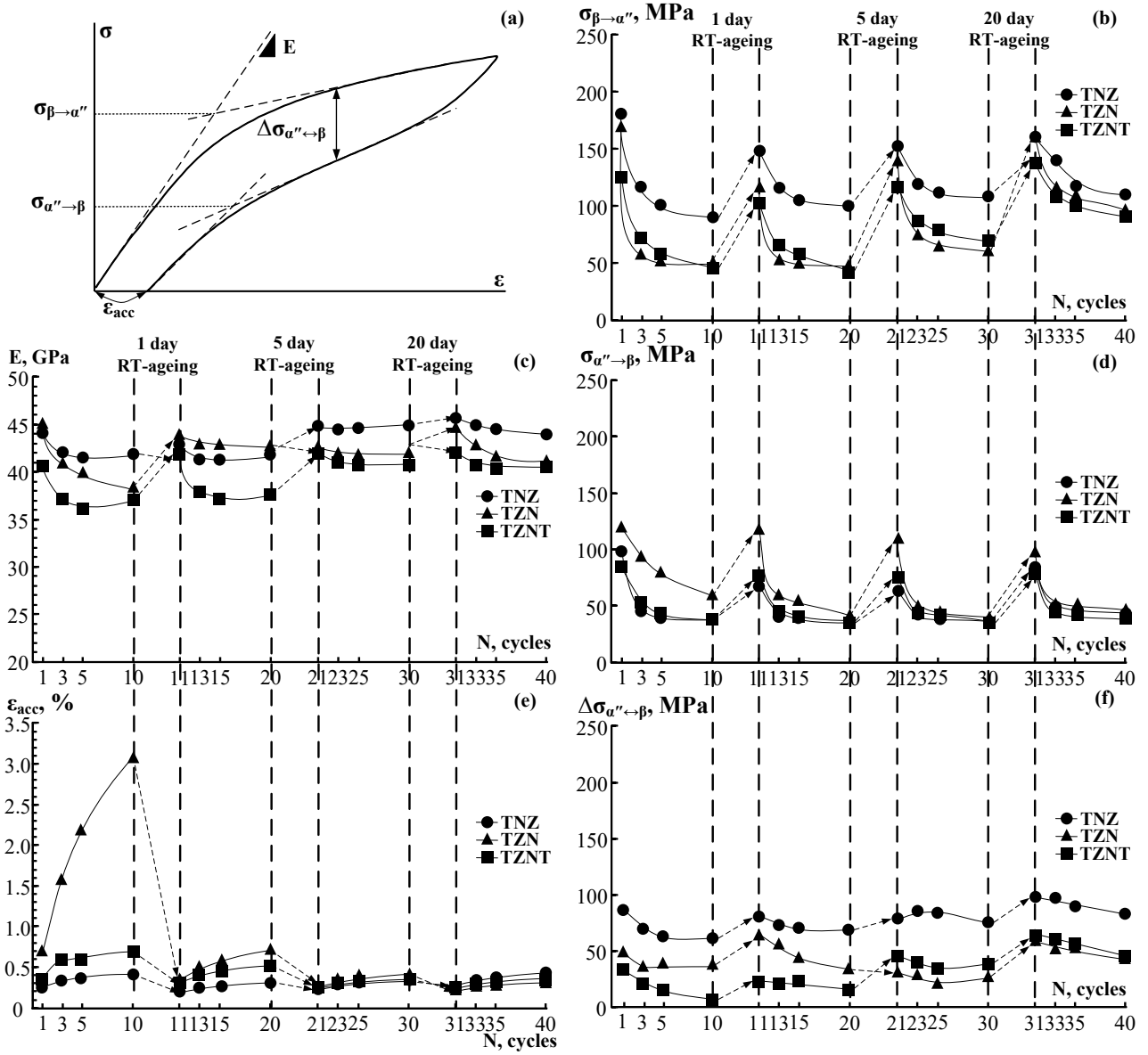

Fig. 3. (a) Controlled parameters of the superelastic loop and their evolution during testing: (b) critical stress for $\beta \rightarrow \alpha''$ transformation, (c) Young's modulus E, (d) critical stress for $\alpha'' \rightarrow \beta$ transformation, (e) accumulated residual strain ε_{acc}, and (f) mechanical stress hysteresis $\Delta\sigma_{\beta \leftrightarrow \alpha}$.

During the initial stage (n=1-10), the $\sigma_{\beta \rightarrow \alpha''}$ decreases gradually during cycling (Fig. 3b). This decrease may have resulted from the generation of favorably oriented micro-stresses of different nature during specimen deformation. Consequently, the plastically deformed α''-phase was stabilized with respect to the parent β-phase, thus decreasing the critical stress required to induce martensitic transformation in the next cycle [9, 15, 16]. However, the drop in $\sigma_{\beta \rightarrow \alpha''}$ was deeper for TZN and TZNT as compared to TNZ. During the second cycling stage (n=11-20), $\sigma_{\beta \rightarrow \alpha''}$ values for all the alloys initially increased and then decreased considerably. It is suggested that the initial increase in $\sigma_{\beta \rightarrow \alpha''}$ for n=11 after one-day room-temperature ageing can be attributed to the precipitation of the isothermal omega phase (ω_{iso}) or to the impurity atoms segregation phenomenon. Since ω_{iso} is rich in Ti-content, it could decrease the martensitic transformation start temperature (M_s of β-phase), which would increase the stress required to induce martensitic transformation [16-18]. However, going from n=12 cycle up to n=20, $\sigma_{\beta \rightarrow \alpha''}$ decreased gradually for all the alloys, which was most probably related to the oriented micro-stress fields generation [15]. For n=21, $\sigma_{\beta \rightarrow \alpha''}$ increased abruptly for all the alloys, and then decreased again during cycling from n=21-30. For n=31, after 20-days room temperature ageing, $\sigma_{\beta \rightarrow \alpha''}$ increased for all the alloys, but this increase was less pronounced for the TNZ alloy than for the TZN and TZNT alloys, which is

attributed to its higher Nb content, and therefore to the lower quantity of isothermal omega phase (ω_{iso}) [19]. Starting from n=31, σβ→α″ decreased for all the alloys, a decrease comparable to that during the preceding cycling (n=21-30 cycles). Nevertheless, at all stages of the tensile testing (Fig. 3b), $\sigma_{\beta\rightarrow\alpha''}$ was always higher for TNZ than it was for TZN and TZNT.

It could be observed for all alloys that there was no obvious difference in the behavior of $\sigma_{\alpha''\rightarrow\beta}$. In other words, strain-controlled cycling with subsequent ageing treatment affects $\sigma_{\alpha''\rightarrow\beta}$ to a lower extent than $\sigma_{\beta\rightarrow\alpha''}$ (compare Fig. 3b and Fig. 3d). It should also be noted that TNZ always exhibited higher $\sigma_{\alpha''\rightarrow\beta}$ as compared to TZN and TZNT.

Nonetheless, it can clearly be seen (Fig. 3f) that in the case of n=1, the TNZ alloy specimens exhibited $\Delta\sigma_{\beta\leftrightarrow\alpha''}$ of ~90 MPa, whereas this value was ~50 MPa and ~40 MPa for the TZN and TZNT alloys. During cycling, TZNT exhibited the best cyclic stability among all the alloys, which makes it highly suitable for functional and superelastic applications in which small stress hysteresis is preferable [3, 9, 17, 18, 20].

Similarly, in the light of their potential medical applications, the levels of the accumulated plastic strains εacc and the Young's modulus stability represent one of the most important parameters to be monitored. It follows from Fig. 3c that the pre-test values of the Young's modulus were close for all the alloys (40-45 GPa). These values decreased to 35-40 GPa during the initial cycling stage (n=1-10). After a one-day RT ageing, the Young's moduli regained their initial values and started to decrease again during the second cycling stage (n=11-20), however at a lower extent. Finally, later stages of ageing and cycling led to the Young's modulus stabilization at initial levels.

In summary, TNZ and TZNT alloys demonstrated stable superior superelastic behavior during all series of cycles, characterized by low levels of accumulated strains εacc (Fig. 3e). In the first cycling series, the accumulated strain ε_{acc} was significantly higher for TZN than for TNZ and TZNT. In the second cycling series, the ε_{acc} decreased rapidly, and the TZN alloy exhibited perfect superelastic behavior during subsequent cycling tests.

2.2 Structure evolution

The main phase constituent in all the alloys studied, irrespective of the testing stage, was β-phase (Fig. 4). The first series of the multicycle testing (Fig. 2) path led to the appearance of a significant amount of residual plastic strain which most likely stemmed from the stress-induced α''-martensite in TZN alloy (see experimental point 2, Fig. 4b). It is well known that this so-called "retained" martensite is a consequence of an imperfect superelastic behavior during tensile testing, which involves the stress-induced martensite formation and its incomplete reverse transformation [1-4]. On the other hand, the pauses alternating the cycling steps were not accompanied by any significant changes in the β- and α''-phase lines' intensities (Fig. 4b, experimental points 3-5).

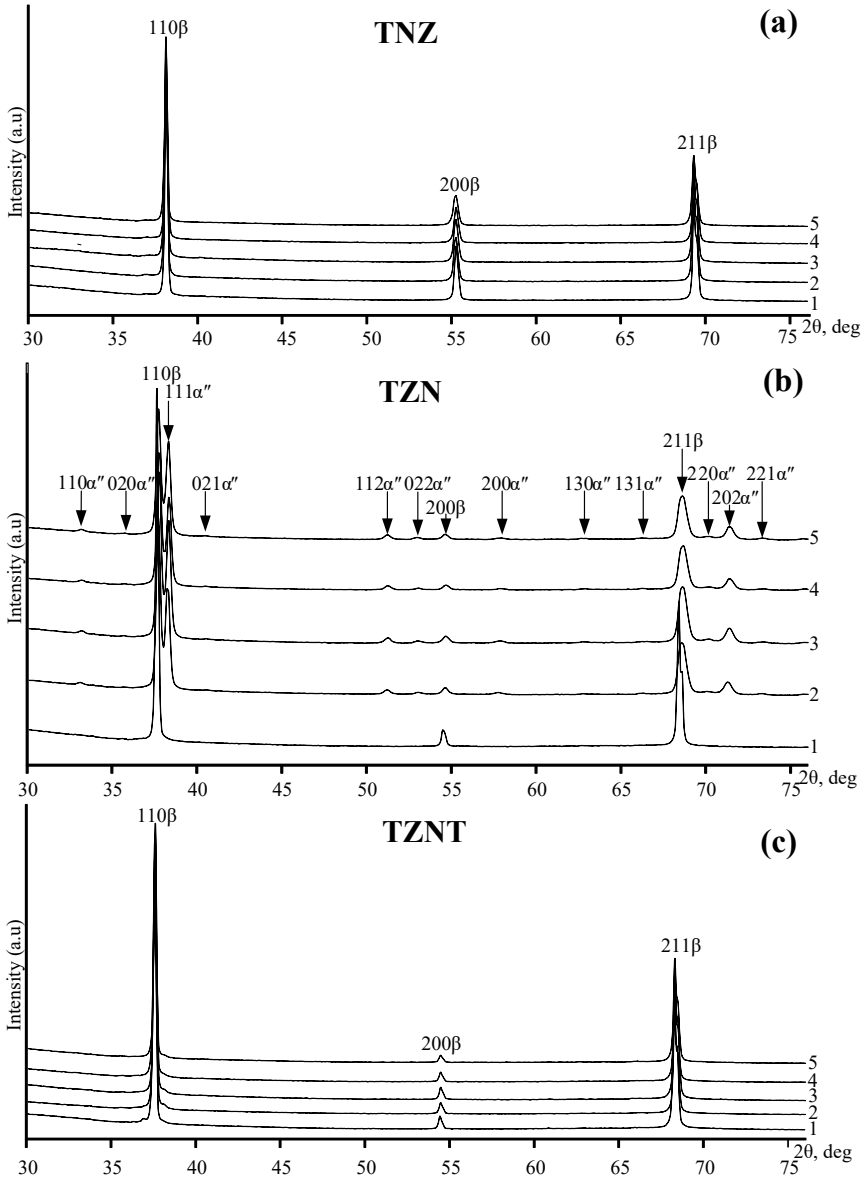

Fig. 4. X-ray diffractograms of (a) TNZ, (b) TZN and (c) TZNT alloys (1-5 corresponds to control points of Figure 1)

The β-phase {200} and {211} X-ray line width values (B_{hkl}) for all alloys in their initial state and after each cycling series are also compared in Table 1. Particularly, in the case of TZN, the first cycling series resulted in a significant increase in the X-ray lines width. This line broadening reflects an accumulation of significant micro-stresses and is a direct consequence of two superimposed phenomena: a) increase in dislocation density caused by true plastic deformation accompanying repetitive $\beta \leftrightarrow \alpha''$ transformations, and b) reorientation of the stress-induced α''-martensite (combination of the "deformation" and "transformation-induced hardening" phenomena) [15].

The accumulation of the longitudinally-oriented tensile micro-stresses near the specimen surface after the first cycling series is revealed through a decrease in the measured β-phase lattice parameters in the case of TZN alloy (Table 1). This result is a consequence of a decrease in the β-phase interplanar distances between the crystallographic planes which are parallel to the specimen surface. Note that no accumulation of the oriented residual micro-stresses was observed in TZNT, and that accumulation was weak in TNZ, due to their much more perfect superelastic behavior starting from the very first cycles (Fig. 2). For the TZN alloy, the theoretical limit of the recovery strain corresponds to 5.5-6% for the entire experiment (Table 1).

Table 1. Structure parameters determined from the X-ray diffractograms

Exp. point	TNZ			TZNT			TZN			
	a, Å	B_{hkl}, 2θdeg		*a*, Å	B_{hkl}, 2θdeg		*a*, Å	ε_{max}, %	B_{hkl}, 2θdeg	
		200	211		200	211			200	211
1	3.3068 ±0.0009	0.26 ±0.02	0.31 ±0.02	3.3430 ±0.0009	0.21 ±0.02	0.30 ±0.02	3.3416 ±0.0004	-	0.30 ±0.02	0.32 ±0.02
2	3.3036 ±0.0006	0.31 ±0.02	0.31 ±0.02	3.3441 ±0.0010	0.22 ±0.02	0.31 ±0.02	3.3382 ±0.0007	5.61 ±0.15	0.42 ±0.03	0.61 ±0.04
3	3.3037 ±0.0009	0.31 ±0.02	0.31 ±0.02	3.3431 ±0.0007	0.25 ±0.02	0.31 ±0.02	3.3378 ±0.0020	5.73 ±0.16	0.44 ±0.03	0.60 ±0.04
4	3.3054 ±0.0012	0.32 ±0.02	0.34 ±0.02	3.3435 ±0.0009	0.25 ±0.02	0.3 ±0.02	3.3383 ±0.0015	5.83 ±0.19	0.46 ±0.03	0.61 ±0.04
5	3.3039 ±0.0010	0.37 ±0.02	0.34 ±0.02	3.3438 ±0.0013	0.28 ±0.02	0.31 ±0.02	3.3386 ±0.0007	5.79 ±0.16	0.42 ±0.03	0.59 ±0.04

Conclusions

The effect of room temperature ageing on the phase composition, mechanical and superelastic properties of the thermomechanically treated Ti-22Nb-6Zr, Ti-18Zr-14Nb, and Ti-18Zr-13Nb-2Ta (at. %) shape memory alloys has been investigated. The following points can be emphasized:

1. ‘Mechanical behavior features observed during the alternating superelastic cycling-RT-ageing testing series were found to be very sensitive to the alloy composition and intermediate ageing.
2. Among the tested alloys, the Ti-Zr based alloy exhibited superior cyclic stability with narrower stress hysteresis as compared to Ti-Nb alloy.
3. TNZ and TZNT demonstrated superior mechanical properties under the combined effect of ageing and mechanical cycling as compared to TZN, due to their lower Young’s moduli and smaller accumulated residual strains with increasing number of cycles.

Acknowledgment

This work was carried out with the financial support of the Ministry of Education and Science of the Russian Federation (project ID RFMEFI57517X0158 and the Natural Science and Engineering Research Council of Canada (NSERC).

References

[1] S. Miyazaki, H.Y. Kim, H. Hosoda, Mater. Sci. Eng. A 438-440 (2006) 18.

[2] H.Y. Kim, S. Miyazaki, Shap. Mem. Superelasticity 2 (2016) 380.

[3] S. Prokoshkin, V. Brailovski, S. Dubinsky, Y. Zhukova, V. Sheremetyev, A. Konopatsky. K. Inaekyan, Shap. Mem. Superelasticity 2 (2016) 130.

[4] V. Brailovski, S.D. Prokoshkin, M. Gauthier, K. Inaekyan, S. Dubinskiy, M. I. Petrzhik, M. Filonov, Mat. Sci. and Eng. C 31(3) (2011) 643.

[5] M. Niinomi, J. Mech. Beh. Biomed. Mater. 1 (2008) 30.

[6] T.W. Duerig, J. Albrecht, D. Richter, P. Fischer, Acta Metall. 30 (1982) 2161.

[7] M.F. Ijaz, H.Y. Kim, H. Hosoda, S. Miyazaki, Mater. Sci. Eng. C 48 (2015) 11.

[8] P. Castany, A. Ramarolahy, F. Prima, P. Laheurte, C. Curfs, T. Gloriant, Acta Mater. 88 (2015) 102.

[9] M. Tahara, H.Y. Kim, H. Hosoda, S. Miyazaki , Acta Mater. 57 (2009) 2461.

[10] V.Sheremetyev, V.Brailovski, S.Prokoshkin, K.Inaekyan, S.Dubinskiy, Materials Science and Engineering C, 58 (2016) 935-944.

[11] A.S. Konopatsky, S.M. Dubinskiy, Yu.S. Zhukova, V. Sheremetyev, V. Brailovski, S.D. Prokoshkin, M.R. Filonov, Materials Science and Engineering A 702 (2017) 301.

[12] S.D. Prokoshkin, V. Brailovski, A.V. Korotitskiy, K. Inaekyan, S.M. Dubinskiy, M.R. Filonov, M.I. Petrzhik, J. Alloys Compd. 577S (2013) 418.

[13] J.B. Nelson, D.P. Riley, Proc. Phys. Soc. 57 (1945) 160.

[14] S.D. Prokoshkin, V. Brailovski, K. Inaekyan, A.V. Korotitskiy, A. Kreitcberg. In: N. Resnina, V. Rubanik (Eds.), Shape Memory Alloys: Properties, Technologies, Opportunities Trans Tech Publication (2015) 260.

[15] V. Sheremetyev, S.D. Prokoshkin, V. Brailovski, S.M. Dubinskiy, A.V. Korotitskiy, M.R. Filonov, M.I. Petrzhik, Phys. Met. Metallogr. 116 (4) (2015) 413.

[16] J. Ma. Karaman I, H.J. Maier, Y.I. Chumlyakov, Acta Mater. 58 (2010) 2216.

[17] Y. Al-Zain, Y.Sato, H.Y. Kim, H. Hosoda, T.H. Nam, S. Miyazaki, Acta Mater. 60 (2012) 4237.

[18] M.F. Ijaz, H.Y. Kim, H. Hosoda, S. Miyazaki, Scripta Mater. 72-73 (2014) 29.

[19] T. Yoneyama, S. Miyazaki, Shape Memory Alloys for Biomedical Applications, Woodhead Publishing, Cambridge, 2009.

[20] S . Miyazaki, T. Imai, Y . Igo, K. Otsuka, Metall Trans. A 17 (1986) 115.